Cement & Concrete Composites 31 (2009) 461–469

Contents lists available at ScienceDirect

Cement & Concrete Composites

journal homepage: www.elsevier.com/locate/cemconcomp

Simulation of capillary shrinkage cracking in cement-like materials

V. Slowik *, T. Hübner, M. Schmidt, B. Villmann

Leipzig University of Applied Sciences, PF 301166, 04251 Leipzig, Germany

ARTICLE INFO

Article history:
Received 27 September 2008
Received in revised form 6 May 2009
Accepted 7 May 2009
Available online 15 May 2009

Keywords:
Early age concrete
Early age cracking
Shrinkage
Interparticle forces
Capillary pressure
Particle model
Discrete modeling

ABSTRACT

In drying suspensions, water loss leads to a capillary pressure build-up in the liquid phase. This effect may also be observed in fresh cement-based materials subjected to evaporation at an open surface. If under decreasing water content the near-surface solid particles are no longer covered by a plane water film, menisci develop along with an associated build-up of negative capillary pressure, resulting in shrinkage and possibly in cracking. A 2D model for simulating the described physical process is presented. For arranging the particles in the 2D specimen a stochastic–heuristic algorithm is used. Subsequently, the course of the water front between the particles is calculated by assuming a constant curvature of the water surface. Particle mobility is taken into account by adopting interparticle forces and performing equilibrium iterations. The model allows one to study the influences of the particle size distribution as well as of the properties of the liquid phase on the capillary pressure build-up and on the cracking risk.

1. Introduction

Concrete members may crack already within the first few hours after casting. At this early age, the material has not reached a significant strength yet and it may be regarded as a drying suspension rather than a solid material. The predominant reason for volume changes and cracking at this age are the capillary forces built up in the liquid phase of the material leading to the so-called capillary shrinkage [1,2]. It is also referred to as plastic shrinkage since it is observed when the cement-based material is still in its plastic stage. Resulting damage is usually in the form of cracks that appear in a relatively regular pattern, see Fig. 1. Such early age cracks occur predominantly in concrete floors and slabs where the upper surface is subjected to a high evaporation rate. The cracks shown in Fig. 1 were formed in a concrete slab on grade probably when the material was still in its plastic stage. Capillary shrinkage cracks may have widths of up to 2 mm and depths of up to 10 cm in thick members [2]. In slabs, they may run through the whole depth of the member [3]. Normally, capillary shrinkage cracks are considerably deeper than those formed by drying induced hygral gradients in hardened concrete [4]. During construction work, early age cracks are sometimes superficially covered by using surface smoothing equipment. However, these cracks tend to open observably under tensile stresses occurring during the hardening or at later ages [2,5]. They may influence the durability of the structure [4]. Crack patterns detected during the service life of concrete members are sometimes quite similar to those formed by capillary shrinkage and may only be explained satisfactorily by taking into account the early age material behavior. Although the physical process leading to capillary shrinkage cracking is well known in the concrete research community and has been investigated experimentally [1,3,5–9], its practical consequences are frequently disregarded in concrete technology leading to extra construction expenses for evaluation and repair [10].

Fig. 2 schematically shows the process of capillary pressure build-up in a drying suspension. A more detailed description as well as corresponding experimental observations may be found in a previous paper [7]. In the material considered here, the solid particles may be either cementitious or inert since the physical process explained in the following discussion takes place in both types of materials [1,2,7]. The liquid phase consists mainly of water. When the material is cast into a form, bleeding may occur, i.e. the solid particles settle due to gravitational forces and on the surface a plane water film is formed (Fig. 2A). Evaporation at the upper surface continuously reduces the thickness of the water film and, eventually, the near-surface particles are no longer covered by a plane water surface (Fig. 2B). Adhesive forces and surface tension result in a curved water surface. Menisci are formed between the solid particles and a negative water pressure is built up. The latter depends on the water surface tension γ and on the main radii R of the curved water surface, i.e. maximum R_1 and minimum R_2 of the radius of curvature, as expressed by the Gauss–Laplace equation.

$$p = -\gamma\left(\frac{1}{R_1}+\frac{1}{R_2}\right) \tag{1}$$

* Corresponding author. Tel.: +49 341 3076 6261; fax: +49 341 3076 7045.
E-mail address: slowik@fbb.htwk-leipzig.de (V. Slowik).

0958-9465/$ - see front matter © 2009 Elsevier Ltd. All rights reserved.
doi:10.1016/j.cemconcomp.2009.05.004

Fig. 1. Early age shrinkage cracks in a concrete slab on grade.

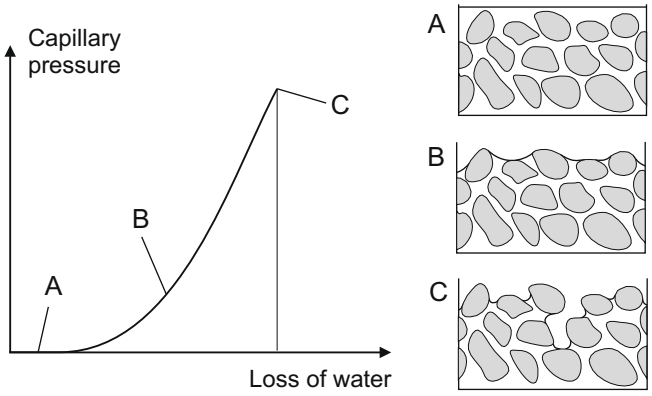

Fig. 2. Capillary pressure build-up in a drying suspension.

In the vicinity of the surface, i.e. up to a depth of at least 10 cm, the water pressure within the interconnected pores is almost uniformly distributed [3]. Fig. 3 shows the capillary pressure measured at several sensor positions. The curves obtained for different distances from the surface follow almost the same path. The maximum absolute pressure values, however, are different. Hydrostatic pressure differences, in this case 0.2 kPa between the sensor positions at depths of 2 cm and 4 cm, respectively, are small when compared to the absolute capillary pressure values.

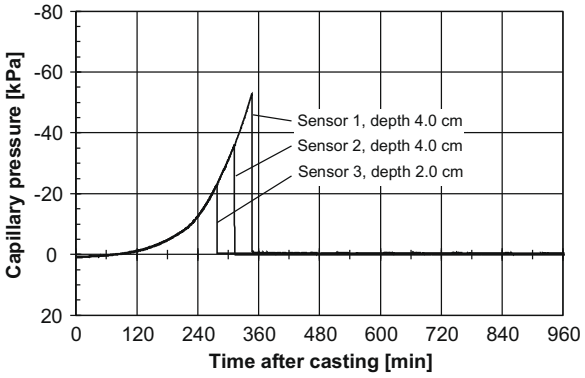

Fig. 3. Capillary pressure at different sensor positions in a concrete specimen with a thickness of 6 cm.

In cementitious materials, the hydration may be an additional cause for the water loss leading to the described capillary pressure build-up [5]. This is of relevance especially for low water–cement ratios.

The negative capillary pressure acts on the particle faces and causes a reduction of the specimen volume. This results first in a settlement or vertical shrinkage strain [2] and later, after the sample is separated from the side faces of the form or cracked, in a horizontal shrinkage strain [7]. The continuing capillary pressure build-up, however, cannot be prevented by the reduction of the interparticle distances. Up to this stage, the specimen volume change is almost equal to the volume of the evaporated water [2,7]. If a certain pressure is reached, the largest gaps between the particles at the surface can no longer be bridged by the menisci and air penetrates locally into the pore system accompanied by a local pressure break-down (Fig. 2C). The pressure value at the first event of air penetration into the pore system is referred to as the air entry value [7,11]. Due to the irregular particle arrangement, the air does not penetrate into all the surface pores simultaneously. The latter are drained successively starting with the larger ones. Therefore, when measuring the capillary pressure at different locations, the corresponding break-down values, i.e. the maximum absolute pressure values, are different and depend on the individual sensor positions. In addition, the capillary pressure might break down locally due to air bubbles reaching the sensor tip [3]. Fig. 4 shows measured pressure versus time curves for different sensor positions at the same depth as well as the corresponding specimen deformations starting from the time of casting. The experimental set-up described in [7] and [10] has been used. It may be seen that the different pressure curves follow the same path as long as the sensor tip is in contact with the pore water. The pressure break-

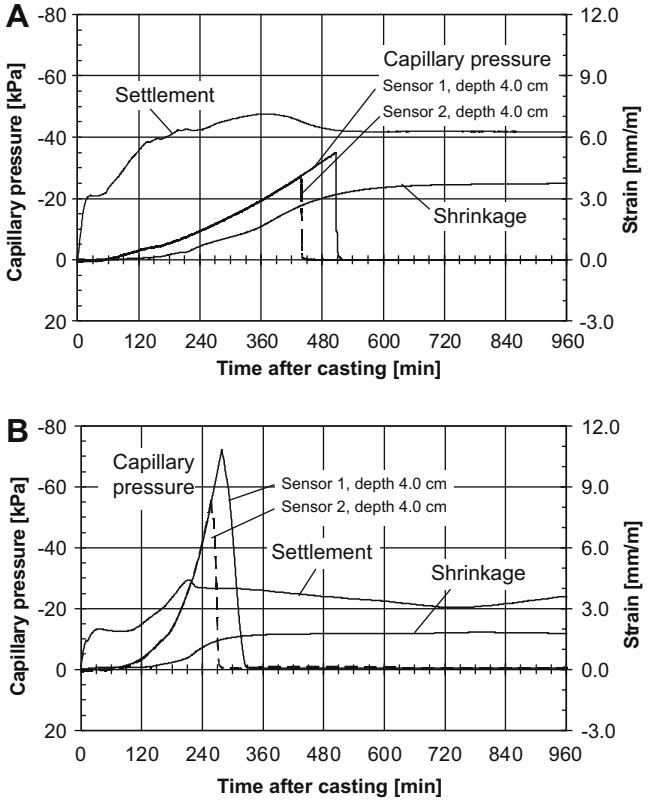

Fig. 4. Capillary pressure, vertical (settlement) and horizontal (shrinkage) strain versus time in a suspension made of fly ash and water (A) and in cement paste (B), specimen thickness 6 cm, identical drying conditions.

down values, however, are different and not representative for the material [3,5].

It has to be considered that in the regions air has penetrated into, the solid particles remain connected by water sleeves in which the negative pressure continues to rise [1]. However, the resulting contracting forces are not increasing proportionally to the pressure since with decreasing main radii of the water surface the pressurized surface area of the particles is also getting smaller.

Due to the non-uniform air penetration, the water pressure might impose resultant forces on the particles with components parallel to the specimen surface where evaporation takes place. Thus, the "breaches" formed by air entry are widened and the neighboring material is compacted. This strain localization might eventually lead to visible cracks. When the pressure reaches the air entry value, the cracking risk is high because the air filled pores are weak points on the specimen surface. The causality between air entry and cracking has been demonstrated by electron microscopic observations [7] as well as by force measurements [4]. In drying suspensions, cracking requires air entry. However, air entry does not necessarily result in cracking. For the latter, sufficient particle mobility is also a prerequisite.

It has been shown that by controlling the capillary pressure build-up the risk of cracking at an early age, i.e. within the first about 6 h after casting, may be reduced significantly [4]. In the following, the term *capillary pressure* is used for the absolute value of this quantity.

A method of closed-loop controlled concrete curing has been proposed which is based on the in situ measurement of the capillary pressure [4,10]. If this pressure reaches a previously defined threshold value, the concrete surface is rewetted and, consequently, the pressure decreases. The threshold value needs to be lower than the air entry value in order to prevent cracking. By using a closed control circuit, it is possible to terminate the rewetting before the capillary pressure becomes zero. In this way, the development of a continuous water film on the concrete surface is prevented. Adding too much water might have an unfavorable effect on the surface quality of the concrete member.

The method of controlled rewetting requires an upper threshold value for the capillary pressure which should be equal to the air entry value of the specific material reduced by an appropriate safety margin. It appears to be possible to identify the air entry value as a material parameter in laboratory experiments. Under continuous water loss, reaching the air entry value is in certain tests accompanied by an increasing deviation between specimen volume change and evaporating water volume, by a temporary maximum of the settlement as well as by a sudden drop of electrical conductivity [7].

The numerical simulation of the drying process would be an alternative way of determining a critical capillary pressure value. As an intermediate step on the way towards this type of analysis, the work presented here was undertaken. It is based on two major simplifications. Firstly, the simulation approach is limited to two dimensions and, secondly, it does not account for chemical reactions in the cement paste which would result in age-dependent properties of the liquid phase and of the solid particles. Hence, the proposed model may be considered to be adequate for inert materials such as suspensions consisting of water and fly ash. The latter is characterized by spherical particles shapes and, correspondingly, circular particles are assumed in the 2D model presented here. The particle sizes of cement and fly ash are for the most part in the same order of magnitude.

Despite its simplifications, the model allows the demonstration of some early age effects occurring in cementitious materials. Capillary pressure build-up, early age shrinkage and cracking are not only dependent on the water evaporation rate but also on the material composition, on the specimen geometry and on mechanical constraints. The air entry value as a material property of the suspension depends on the particle size distribution, on the particle content, on the air content as well as on the mobility of the particles. The latter has also a significant influence on strain localization and cracking. The presented model allows one to study some of these influences and to discuss them with regard to the early age cracking risk.

2. Description of the model

2.1. Generation of the 2D geometrical model and simulation of drying

The model consists of circular solid particles dispersed in a liquid phase. In the study presented here, all specimens had a rectangular shape. For allocating the particles inside the specimen, a stochastic–heuristic algorithm was used which had been originally developed for generating concrete mesolevel models [12,13]. According to this algorithm, the particles are consecutively placed in the specimen starting with the largest ones. The initial position of the respective particle is randomly chosen. If the latter overlaps previously located ones or the specimen boundaries, several attempts of translational movements are undertaken until an acceptable position has been found. This strategy allows higher particle volume contents and requires significantly shorter computing times than purely stochastic algorithms.

It has to be considered that the particle size distributions in a 3D specimen and in a 2D section of the same are not identical since not all the spheres are cut centrically. This discrepancy was disregarded here, i.e. the diameters of the circles in the 2D model were assumed to be the same as those of the real particles. By adopting this simplification, the particle diameters in the 2D model are about 15% larger on average than those of the actual spheres (diameter of a section through the quarter point of a sphere with unit diameter = $\sin(60°) \approx 0.866$). However, in this way the interparticle forces were obtained for the real particle diameters.

In the simulation of the drying process, the water content of the system is continuously decreasing. As stated before, this water loss may lead to the formation of menisci in the water front between the particles and to the corresponding capillary pressure build-up. For computational reasons, in the presented simulations the water pressure served as a control parameter and was increased incrementally. Accordingly, for each pressure increment the course of the water front was calculated by assuming constant surface curvature between adjacent surface particles and a wetting angle of zero, see Fig. 5. Once the water front had been determined for a given pressure, the water volume in the specimen could be calculated. Here, the 2D simplification again caused some difficulties. It was decided to determine the water pressure for a double-curved surface with constant radius r.

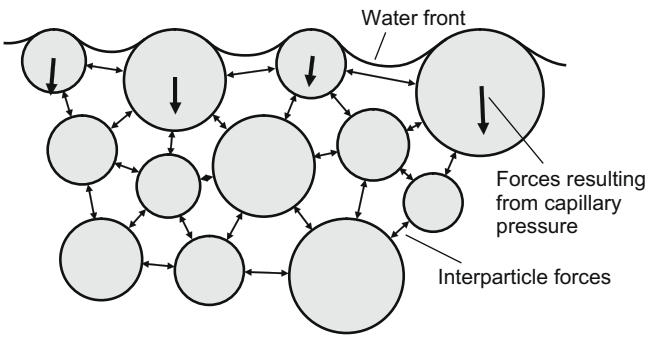

Fig. 5. Forces acting on solid particles: interparticle and capillary forces, gravitational forces not shown.

$$p = \frac{2\gamma}{r} \tag{2}$$

The forces resulting from this pressure, see Fig. 5, were calculated under the assumption of spherical particles, i.e. the pressure was acting on the surface of spherical caps. Gravitational and uplift forces were also determined for spherical particles. However, the water volume in the system was calculated on the basis of the 2D model assuming unit thickness, i.e. the solid particles were regarded as cylinders. These assumptions were considered to be appropriate in view of the 2D model simplification.

2.2. Interparticle forces

The interaction between the solid particles is described by interparticle forces, see Fig. 5, whereby only those between neighboring particles are considered, i.e. between particles separated exclusively by a liquid interlayer. This simplification is justified by the comparably strong decrease of the interparticle forces with increasing particle distance. Fluid viscosity as well as inertia of the solid particles is neglected because of the low particle velocity. Furthermore, frictional forces are disregarded since the spherical solid particles do not have direct contact.

The interparticle forces considered here include van-der-Waals and electrostatic forces. They depend on particle distance and radii as well as on the physical and chemical properties of the solid and liquid phases. By superimposing the different types of physical interaction a resulting interparticle force is obtained, see Fig. 6, which is also referred to as disjoining pressure [14,15]. This resulting interparticle force effectively describes the complex interaction between two solid particles and the liquid interlayer.

The van-der-Waals force comprises several types of interaction between electrically neutral particles and is always attractive between surfaces of the same material. Flatt [16,17] proposed the simplified approach according to Eq. (3) where r are the particle radii, a the particle distance and A_H the Hamaker constant. The latter is a material property and, according to Flatt [17], for cement-like materials nearly linearly dependent on the solid density. The simplified calculation according to Eq. (3), which was adopted for the simulations presented here, is justified for cementitious suspensions which are characterized by high ion concentrations in the pore solution and small particle distances [16].

$$F_{vdW} = A_H \cdot \frac{R}{12 \cdot a^2} \text{ with } R = \frac{2 \cdot r_1 \cdot r_2}{r_1 + r_2} \tag{3}$$

For determining the electrostatic force, Eq. (4) is used which was also proposed by Flatt [18]. This force describes the repulsion of the ion clouds which are surrounding particles in aqueous solutions. It strongly depends on the properties of the liquid phase, especially on the ion concentration and on the pH value. In Eq. (4), ε_0 is the vacuum permittivity, ε_r the relative permittivity of water, ζ the zeta-potential, k_B the Boltzmann constant, T the absolute temperature, e the elementary charge, z_+ the valence and n_+^b the concentration of an equivalent symmetric electrolyte. The parameter δ is the so-called Debye length.

$$F_{el} = -2 \cdot \pi \cdot \varepsilon_0 \cdot \varepsilon_r \cdot \zeta^2 \cdot R \cdot \frac{1}{\delta} \cdot \frac{e^{-\frac{a}{\delta}}}{1 + e^{-\frac{a}{\delta}}} \text{ with } \delta = \sqrt{\frac{\varepsilon_0 \cdot \varepsilon_r \cdot k_B \cdot T}{2 \cdot e^2 \cdot z_+^2 \cdot n_+^b}} \tag{4}$$

Once the van-der-Waals and electrostatic forces are known, the resulting interparticle force F_{res} may be calculated.

$$F_{res} = F_{vdW} + F_{el} \tag{5}$$

In addition to the electrostatic and van-der-Waals forces, there are other types of interaction between particles in aqueous solutions which are not explicitly considered in the model. The effect of the Brownian motion on the solid particles may be neglected since the considered particle sizes are too large. If polymer-based superplasticizers are used, additional repulsive and far-reaching steric forces hinder the close approach of particles. Steric forces have not been taken into account yet, but may be implemented in the model. Solvation forces as the structural component of the disjoining pressure [15] result from the orientation of the water molecules surrounding solid particles. It becomes significant only for short particle distances and may be considered to be included in the simplified approach used here. In addition, the interaction of the adjacent electron clouds causes the so-called Born repulsion which also is of relevance only for very small particle distances.

Although approaches for the quantitative determination of the last mentioned near-field repulsive forces have been proposed, they are not directly implemented in the model presented here. The description of the short-distance particle interaction rather depends on requirements given by the numerical solution method. This is not expected to significantly affect the final results since the calculated particle distances are normally larger than those at which solvation and Born forces become decisive. During the iterative solution, however, very short particle distances and even overlapping might occur. As a consequence, in the short-distance and overlapping range a continuous force function with comparably steep slope is adopted, see Fig. 7. This force, although not physically justified, qualitatively resembles the real repulsive force. In the overlapping range, i.e. for negative distances, it may be regarded as a penalty force required for the numerical solution scheme. As a mathematical expression for the assumed short-distance interparticle force, see Fig. 7, a parabolic function, Eq. (6), is used. The considered interparticle force results from Eq. (6) for particle distances smaller than or equal to a_P, which is a multiple of the Debye length, and from Eq. (5) for larger distances. At the transition point a_P, value and slope of the two functions are equal. Based on this condition, the coordinates of the parabola vertex ($a_{P,S}$; $F_{P,S}$) may be calculated if a distance a_P and a shape parameter f_P are assumed.

$$F_P = -f_P \cdot (a - a_{P,S})^2 + F_{P,S} \tag{6}$$

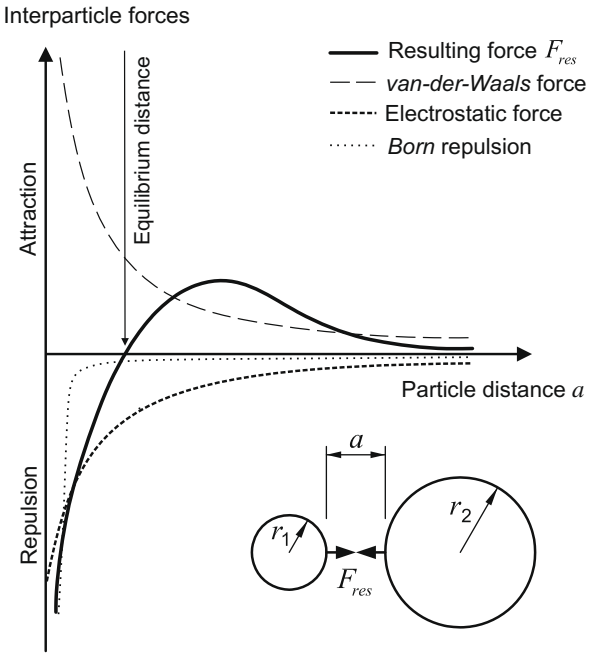

Fig. 6. Interparticle forces versus particle distance.

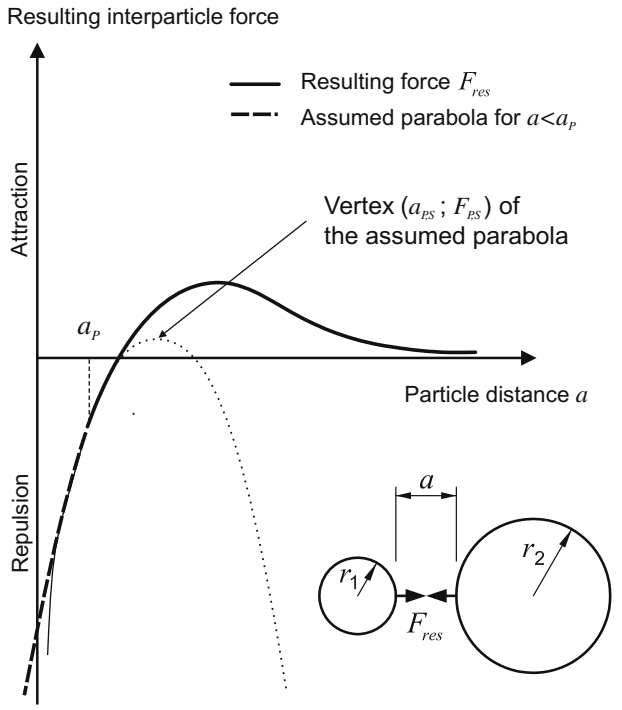

Fig. 7. Assumed curve for interparticle force versus particle distance in the short-distance range.

The 2D simplification of the model requires a modification of the force–distance relationship outlined above. As shown in Fig. 6, the resulting interparticle force is zero at a certain particle distance. This equilibrium distance depends on the solid and fluid properties, but not on the particle sizes. Under the action of external forces, for instance gravitational or capillary forces, the equilibrium distance changes; usually it becomes smaller. In a 2D section of a suspension, the apparent equilibrium particle distances are considerably larger than in the real sample since not all the centroids of the particles are located in the intersecting plane. Out-of-plane interparticle forces are not accounted for in the 2D model. For this reason, the force–distance relationship has to be scaled on the distance axis. For the simulations presented here, this was done by specifying a mean equilibrium particle distance for the 2D model and accordingly calculating a distance scale factor to be used for the determination of interparticle forces. This 2D mean equilibrium particle distance has been derived on the basis of the measurable porosity of real materials. In experiments performed with suspensions made of fly ash and water [19], the initial porosity was 40%. By the time the air entry value was reached it had decreased to about 35%. Consequently, the porosity of the 2D models has been adjusted to this range. Firstly, a comparably uniform particle arrangement was obtained by gradually increasing the minimum particle distance in the stochastic–heuristic model generation, see Section 2.1. After centering the particles with respect to their neighbors, the average particle spacing has been regarded as the mean equilibrium particle distance in the 2D model. For particle sizes ranging from 2 μm to 63 μm a value of 1.5 μm was identified and for those ranging from 4 μm to 32 μm a value of 1.6 μm. These mean equilibrium particle distances were then used in the 2D simulations. It has to be pointed out that the real equilibrium particle distance in a cement suspension calculated on the basis of the physical and chemical properties proposed by Flatt [16] amounts to only 4.3 nm. Using this value in a 2D simulation, however, would result in an unrealistically dense structure which does not resemble the real material. Furthermore, unrealistically high capillary pressure values would be reached in the simulations.

As stated before, the 2D mean equilibrium particle distance was introduced for taking into account the out-of-plane supporting forces acting on the particles. Magnitude and direction of these forces are varying and, therefore, the mean equilibrium particle distance in the 2D model should also show a variance. In the presented simulations, a Gaussian distribution has been adopted with 99.85% of the values being larger than 1% of the mean value. For preventing negative equilibrium particle distances, values smaller than 1% of the mean value were dismissed.

2.3. Iterative solution

Taking into account the forces resulting from capillary pressure as well as gravitational and interparticle forces, a state of equilibrium is searched for by using an implicit solution scheme. The analysis bases on a truss model and the solution is obtained by an iterative matrix stiffness method. In each of the iterations, the connectivities between the particles are updated, a new water front is calculated, see Section 2.1, and the particles are shifted towards directions which minimize the potential energy of the system. For determining the internal portion of the potential energy, the secant slope of the force–distance curve, see Section 2.2, serves as "member" stiffness. When previously set convergence limits are met, the next capillary pressure increment is applied. Several convergence criteria based on particle displacements and unbalanced forces are used. When no water front connecting the side faces of the mould can be found anymore or a further pressure increase does not yield physically sound results, the maximum capillary pressure is considered to be reached and the simulation is terminated.

Fig. 8 shows a model of a drying suspension under increasing capillary pressure, from top to bottom. In the first line, i.e. at zero pressure, all particles (dark circles) are located below the surface of the water (gray). When water is evaporating, menisci are formed in the water front between the particles at the surface and a capillary pressure is built up in the water-filled pore system. This pressure results in downward forces on the superficial particles leading to a settlement of the material. It may be seen that the air entry into the system does not occur everywhere at the same pressure. A local "gap" is formed and widened by the horizontal components of the increasing capillary forces. Eventually, the attracting interparticle forces between the opposite sides of the "gap" have reached a negligible value and a crack has developed. When evaluating the simulation results, this phenomenon of strain localization and separation is regarded as "cracking".

It was found that despite the 2D simplification, numerically determined capillary pressure values are in good accordance with the experimental results. However, the simulation results differ from the experimental findings as far as the evaporated water volume is concerned [7]. This may be attributed to the 2D simplification and also to the very small specimen height in the simulations. In view of the identification of a critical pressure value to be used for controlled concrete curing, the capillary pressure is the more important outcome of the simulations when compared to the evaporated water volume.

3. Numerical simulations and discussion of the results

In parametric studies, several influences on capillary pressure and early age cracking risk were investigated [20]. Table 1 contains the standard set of input parameters used in these simulations. As stated before, the force–distance curve was scaled on the distance axis in order to adjust the mean equilibrium particle distance to the values mentioned in Section 2.2. As results of the simulations, images showing particle arrangement and water front as well as the capillary water pressure versus water loss curves were evaluated.

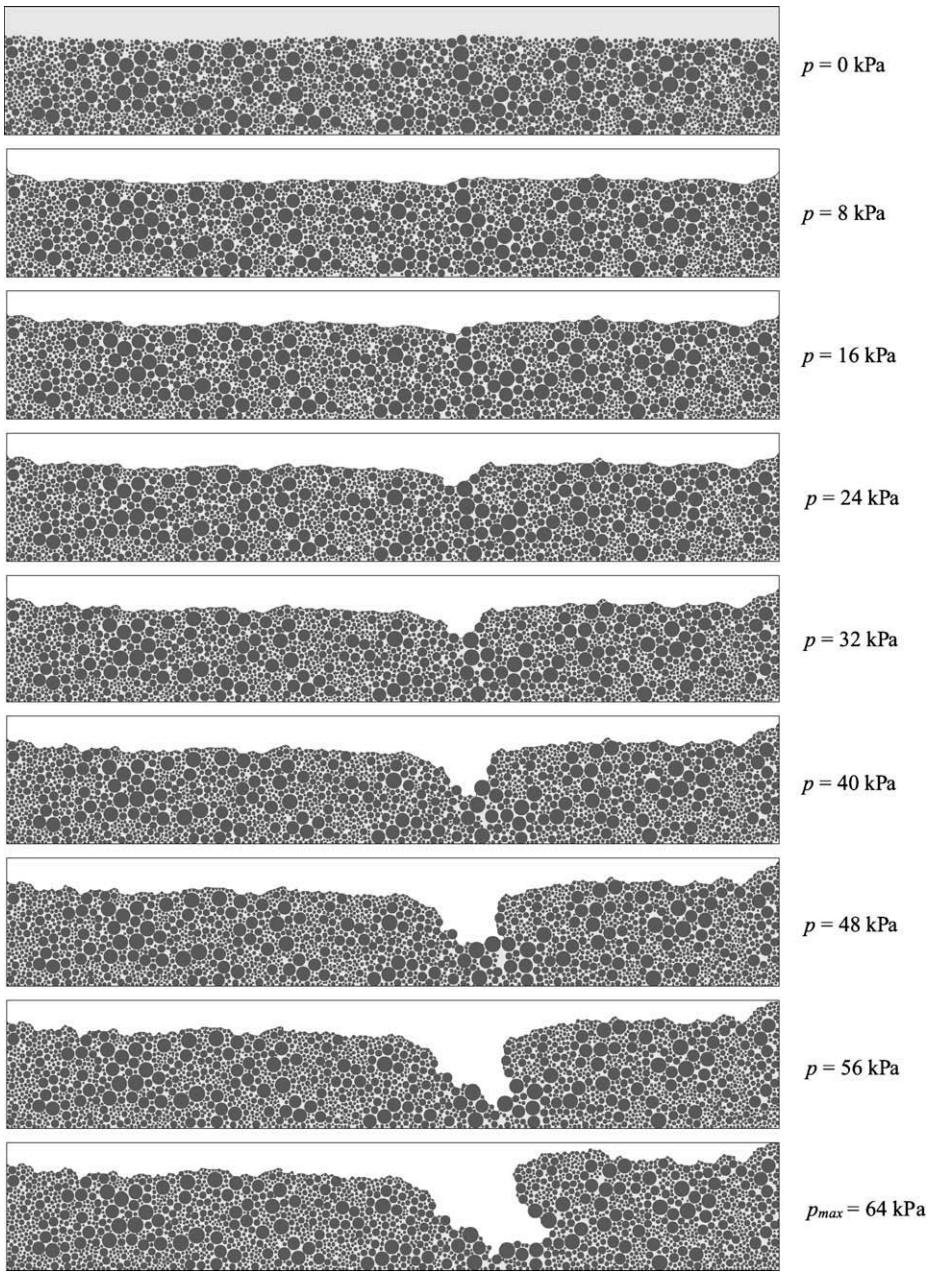

Fig. 8. Simulation of the capillary pressure build-up in a drying suspension, absolute capillary pressure value p increasing from top to bottom, particle sizes ranging from 4 μm to 32 μm.

Table 1
Material parameters assumed for suspensions made of fly ash and water.

van-der-Waals force	Hamaker constant, $A_H = 2.91 \times 10^{-21}$ J
Electrostatic force	Zeta-potential, $\zeta = -0.035$ V Valence of an equivalent symmetric electrolyte, $z_+ = 3.52$ Concentration of an equivalent symmetric electrolyte, $n_+^b = 16.96$ mol/m^3
Parabola for the short-distance range	Shape parameter[a], $f_P = 10^9$ N/m^2 Transition distance, $a_P = 6.433\ \delta$ (δ ... Debye length)

[a] This parameter is applied to the force–distance curves after they have been scaled on the distance axis for adjusting them to the 2D mean equilibrium particle distance, see Section 2.2.

When varying the specimen dimensions, it was found that the width did not have an influence on the measured pressure–water loss curves. However, a certain minimum width is required for eliminating boundary effects and allowing strain localization.

The specimen height strongly affects the slope of the pressure–water loss curve. An almost linear relationship between height and water loss was observed in the simulations. This effect has been experimentally investigated by Radocea [6] and may be attributed to the height dependent amount of water which is transported from the inner pores to the specimen surface under the action of the consolidating capillary pressure.

In the following, two different effects of the material composition on the behavior of drying suspensions are discussed.

3.1. Influence of the particle size

Shrinkage strain and cracking risk are significantly reduced if the particle sizes are increased. The comparably high self-weight

of the larger particles results in a more stable structure and limits particle mobility. Gravitational forces are in this case large when compared to the interparticle forces. Therefore, the particles tend to rest on each other and remain nearly unmoved under the action of the capillary pressure. Furthermore, the slope of the capillary pressure versus water loss curve is less steep for larger particles because of the increased pore diameters. As far as the effect of gravitational forces on the pressure–water loss curve is concerned, simulations with maximum particle sizes of up to 63 μm have shown that this influence is negligible in the considered range of particle sizes.

Fig. 9 shows drying simulations for suspensions with particle sizes ranging from 4 μm to 32 μm and 40 μm to 320 μm, respectively. Similar size distributions and particle arrangements were used. It may be seen that in the case of the smaller particles strain localization and crack initiation take place whereas in the other case the particle mobility appears to be much smaller and no major cracks are formed. This result corresponds to observations in nature. Capillary shrinkage cracks may be formed for instance in silts but are unlikely to occur in sand with comparably large particle sizes. However, air entry takes place in both types of material.

If the portion of fine particles is increased or if the smallest particle size is decreased, the slope of the pressure versus water loss curve becomes steeper and higher maximum pressure values are reached. These effects may be explained by the smaller spaces between the superficial particles. It was also found that the material tends to be more vulnerable to cracking which may be partially attributed to the higher pressure values, but also to the increased particle mobility. Fine particles are more mobile than larger ones because of their comparably small self-weight. As explained before, this allows a stronger strain localization which may eventually lead to cracking. Fig. 10 shows the drying simulation for a suspension with particle sizes ranging from 2 μm to 63 μm. In general, the simulations with this particle size distribution yielded higher maximum pressure values than those with particle sizes ranging from 4 μm to 32 μm.

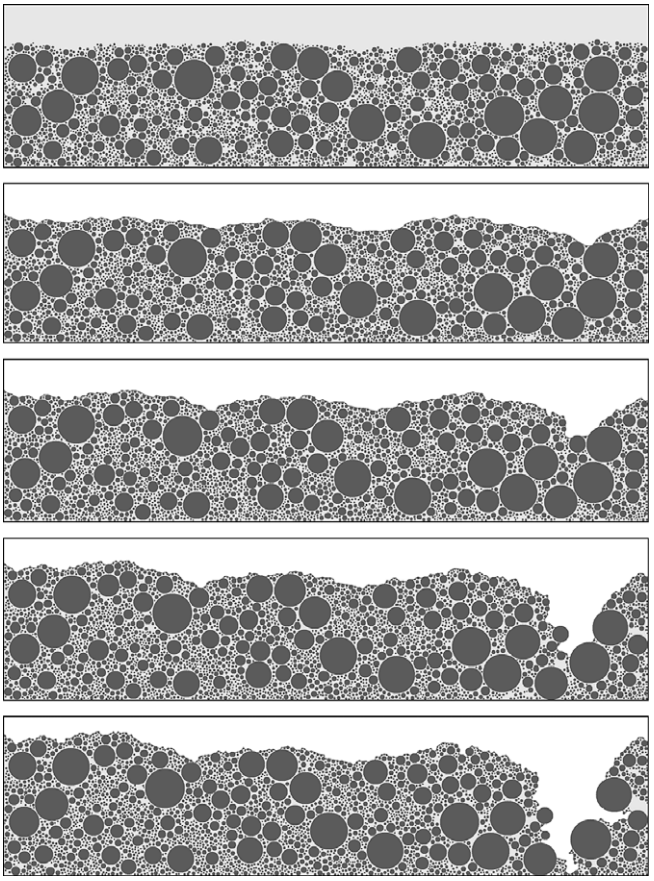

Fig. 10. Simulation of capillary pressure build-up, absolute values from top to bottom: 0 kPa, 24 kPa, 48 kPa, 72 kPa, p_{max} = 88 kPa, particle sizes ranging from 2 μm to 63 μm.

3.2. Influence of the equilibrium particle distance

The equilibrium particle distance, see Section 2.2, also has an effect on the material behavior under drying. It depends on the properties of the solid as well as of the liquid phase. In the case of cementitious materials, it may be influenced by additives like superplasticizers. The equilibrium particle distance affects the behavior of drying suspensions in two different ways. On one hand,

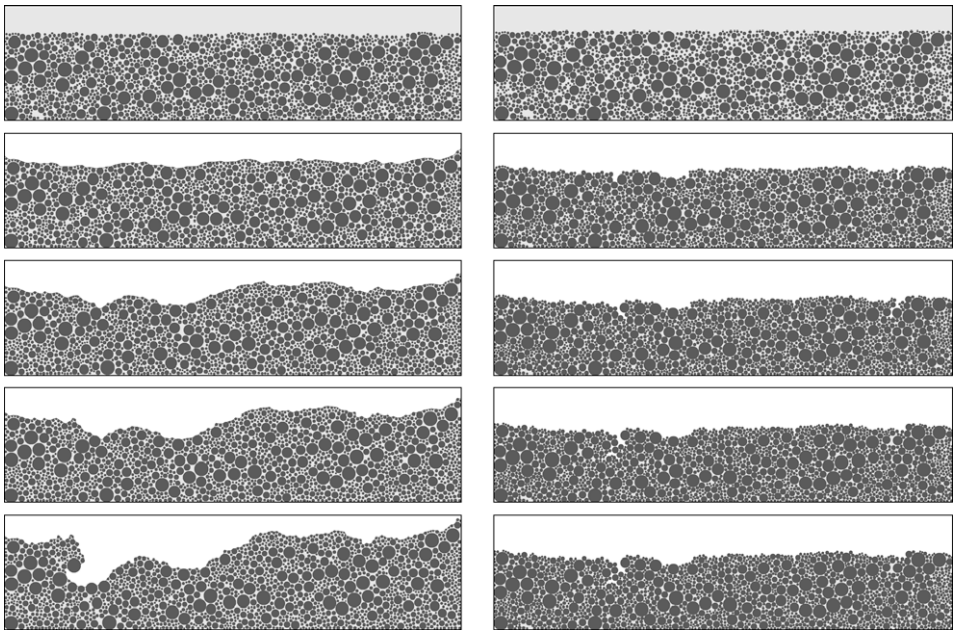

Fig. 9. Simulation of capillary pressure build-up, absolute values from top to bottom: 0 kPa, 16 kPa, 32 kPa, 40 kPa, p_{max}; left: particle sizes ranging from 4 μm to 32 μm, p_{max} = 56 kPa; right: particle sizes particle sizes ranging from 40 μm to 320 μm, p_{max} = 40 kPa.

particle mobility will increase with this distance and, on the other hand, the pressure increase will be less steep. The last mentioned effect results from the wider particle spacing in the case of larger equilibrium distances.

Fig. 11 contains the results of drying simulations with two different mean equilibrium particle distances $a_{0,2D}$, but with the same initial porosity. The upper part of the figure shows the particle arrangement in both simulations under the same capillary pressure of 72 kPa. For the larger mean equilibrium particle distance, "crack" initiation has already occurred at this pressure level. As expected, larger equilibrium distances increase particle mobility and promote crack initiation. When comparing the capillary pressure versus water loss curves, it may be seen that in the case of the small mean equilibrium particle distance a comparably large amount of water needs to evaporate before the capillary pressure decisively increases. This is due to the higher potential for consolidation of the material. Because of the difficulties with the calculated water loss values, see Section 2.3, these values were multiplied by a constant factor of 37 before displaying them in Fig. 11 in order to ease comparisons with measured pressure–water loss curves [7].

The lower part of Fig. 11 shows results of the same simulations. However, when plotting the capillary pressure versus water loss curves, it was assumed that the initial porosity was small enough to prevent further consolidation during the beginning capillary pressure build-up. Accordingly, the curve for the small mean equilibrium particle distance has been shifted in the direction towards zero water loss. Under this assumption, the comparison of the two curves shows the expected steeper slope in the case of small particle distances. For a certain water loss value, i.e. at a certain point in time for a given evaporation rate, the capillary pressure will be higher. As a consequence, strain localization may possibly occur earlier when the equilibrium particle distance is small, see lower part of Fig. 11.

As far as the cracking risk is concerned, the two effects explained above counteract each other. Simulation results have shown, however, that with increasing equilibrium particle distance the material tends to form a more pronounced crack pattern.

4. Concluding remarks

By using a 2D particle model, physical processes taking place in drying suspensions have been numerically simulated. These processes also occur in cement paste at a very early age, i.e. before the material has reached a significant strength. The presented model allows one to simulate the capillary pressure build-up due to water loss, the resulting particle displacements, and possibly crack initiation. These phenomena may also be observed in experiments and their investigation is aimed to a better understanding of capillary shrinkage and cracking. On the basis of the numerical simulations, it is possible to identify several influences on the early age cracking risk and to systematically study their significance.

A number of simplifying model assumptions had to be made, most of them because of the restriction to two dimensions. For a quantitative evaluation of the simulation results, the model would require extensions and refinements. Especially the method of determining a representative value for the evaporated water volume on the basis of the 2D simulation results needs to be improved in order to allow a direct comparison with measured data.

Despite the limitations of the model, some effects of the material composition on the behavior under drying could be demonstrated. The early age cracking risk increases with decreasing particle sizes. As far as the influence of the equilibrium particle dis-

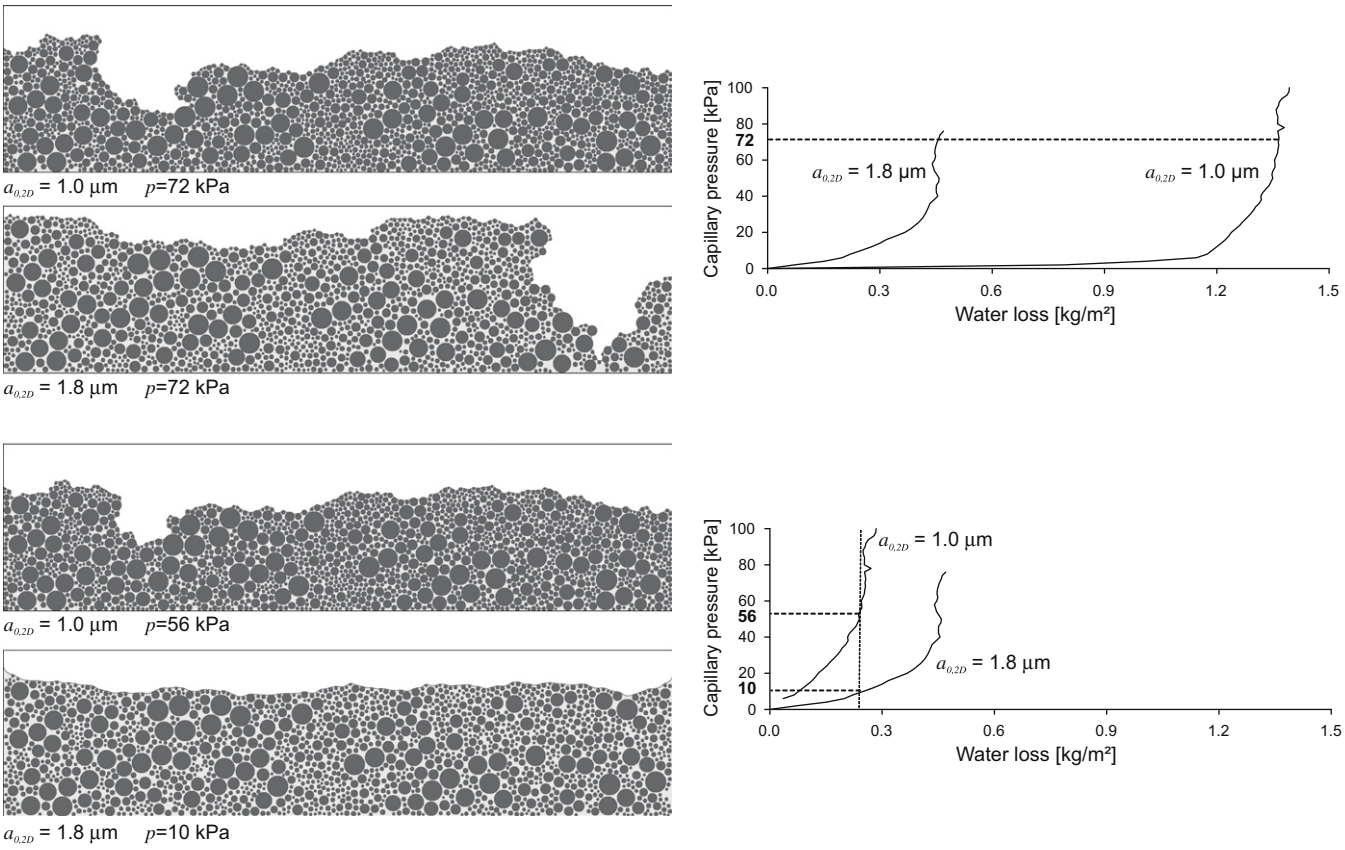

Fig. 11. Simulation of capillary pressure build-up with different mean equilibrium particle distances $a_{0,2D}$, particle sizes ranging from 4 µm to 32 µm, absolute values of capillary pressure are shown.

tance is concerned, a tendency of an increased cracking risk for high equilibrium distances was observed in the simulations.

So far, only the behavior of suspensions with inert solid particles has been simulated. The evolution of particle sizes due to cement hydration and age-dependent properties of the fluid phase have not been considered yet. In future simulations, the effect of additives on early age cracking will also be investigated.

Acknowledgment

The financial support of the research by the Federal Ministry of Education and Research in Germany is gratefully acknowledged.

References

[1] Wittmann FH. On the action of capillary pressure in fresh concrete. Cem Concr Res 1976;6:49–56.
[2] Grube H. Definiton der verschiedenen Schwindarten, Ursachen, Größe der Verformungen und baupraktische Bedeutung. beton 2003;12:598–603.
[3] Esping O, Löfgren I. Cracking due to plastic and autogenous shrinkage – Investigation of early age deformation of self-compacting concrete. Report 2005:11, Department of Civil and Environmental Engineering, Chalmers University of Technology, Göteborg, Schweden; 2005.
[4] Slowik V, Schmidt M, Neumann A, Dorow J. Early age cracking and its influence on the durability of concrete structures. In: Tanabe T, Sakata K, Mihashi H, Sato R, Maekawa K, Nakamura H, editors. Proceedings of the 8th international conference on creep, shrinkage and durability mechanics of concrete and concrete structures (CONCREEP 8), September 30–October 2, 2008, Ise-Shima, Japan, vol. 1. London: Taylor & Francis Group; 2008. p. 471–7.
[5] Holt E, Leivo M. Cracking risks associated with early age shrinkage. Cem Concr Compos 2004;26(5):521–30.
[6] Radocea A. A study on the mechanism of plastic shrinkage of cement-based materials. PhD thesis, Göteborg, Chalmers University of Technology Göteborg; 1992.
[7] Slowik V, Schmidt M, Fritzsch R. Capillary pressure in fresh cement-based materials and identification of the air entry value. Cem Concr Compos 2008;30(7):557–65.
[8] Hammer TA, Fosså KT. Influence of entrained air voids on pore water pressure and volume change of concrete before and during setting. Mater Struct 2006;39(293):801–8.
[9] Sivakumar A, Santhanam M. A quantitative study on the plastic shrinkage cracking in high strength hybrid fibre reinforced concrete. Cem Concr Compos 2007;29(7):575–81.
[10] Schmidt D, Slowik V, Schmidt M, Fritzsch R. Auf Kapillardruckmessung basierende Nachbehandlung von Betonflächen im plastischen Materialzustand (Early age concrete curing based on capillary pressure measurement). Beton-und Stahlbetonbau 2007;102(11):789–96.
[11] Fredlund DG, Rahardjo H. Soil mechanics for unsaturated soils. New York, Chichester, Brisbane, Toronto, Singapore: John Wiley & Sons, Inc.; 1993.
[12] Leite JPB, Slowik V, Mihashi H. Computer simulation of fracture processes of concrete using mesolevel models of lattice structures. Cem Concr Res 2004;34(6):1025–33.
[13] Leite JPB, Slowik V, Apel J. Computational model of mesoscopic structure of concrete for simulation of fracture processes. Comput Struct 2007;85(17–18):1293–303.
[14] Wittmann FH. Heresies on shrinkage and creep mechanisms. In: Tanabe T, Sakata K, Mihashi H, Sato R, Maekawa K, Nakamura H, editors. Proceedings of the 8th international conference on creep, shrinkage and durability mechanics of concrete and concrete structures (CONCREEP 8), September 30–October 2, 2008, Ise-Shima, Japan, vol. 1. London: Taylor & Francis Group; 2008. p. 3–9.
[15] Churaev NV, Derjaguin BV. Inclusion of structural forces in the theory of stability of colloids and films. J Colloids Interf Sci 1985;103(2):542–53.
[16] Flatt RJ. Interparticle forces and superplasticisers in cement suspensions. PhD thesis, Zurich, Swiss Federal Institute of Technology Zurich, No. 2040; 1999.
[17] Flatt RJ. Dispersion forces in cement suspensions. Cem Concr Res 2004;34(3):399–408.
[18] Flatt RJ. Towards a prediction of superplasticized concrete rheology. Mater Struct 2004;37(269):289–300.
[19] Fritzsch R. Zum Austrocknungsverhalten von jungem Beton. Diploma thesis, Leipzig, Germany, Leipzig University of Applied Sciences; 2006.
[20] Hübner T. Zur Simulation der kapillaren Schwindrissbildung in austrocknenden Suspensionen. MSc thesis, Leipzig, Germany, Leipzig University of Applied Sciences; 2007.